Optical Control of Polaritons: From Optoelectronic to Spinoptronic Device Concepts

R. Binder[a,b], S.M.H. Luk[b], N. H. Kwong[a], P. Lewandowski[c], S. Schumacher[c], O. Lafont[d], E. Baudin[d], J. Tignon[d], A. Lemaitre[e], J. Bloch[e], Ch.K.P. Chan[f], and P.T. Leung[f]

[a]College of Optical Sciences, University of Arizona, Tucson, AZ 85721, USA
[b]Department of Physics, University of Arizona, Tucson, AZ 85721, USA
[c]Physics Department and Center of Optoelectronics and Photonics Paderborn (CeOPP), Universität Paderborn, Warburger Strasse 100, 33098 Paderborn, Germany
[d]Laboratoire Pierre Aigrain, École Normale Supérieure, PSL Research University, CNRS, Université Pierre et Marie Curie, Sorbonne Universités, Université Paris Diderot, Sorbonne Paris Cité, 24 rue Lhomond, 75231 Paris Cedex 05, France
[e]Laboratoire de Photonique et de Nanostructures, CNRS Route de Nozay, FR-91460 Marcoussis, France
[f]Department of Physics and Institute of Theoretical Physics, The Chinese University of Hong Kong, Hong Kong SAR, China

ABSTRACT

Exciton-polaritons in semiconductor microcavities have been studied intensely, both with respect to their intriguing fundamental physical properties and with respect to their potential in novel device designs. The latter requires ways to control polaritonic systems, and all-optical control mechanisms are considered to be especially useful. In this talk, we discuss and review our efforts to control the polariton density, utilizing optical four-wave mixing instabilites, and the spin or polarization textures resulting from the optical spin Hall effect. Both effects are readily observable in the cavity's far-field emission, and hence potentially useful for optoelectronic and spinoptronic device applications.

Keywords: Polaritons, semiconductor microcavities, optical switching, optical spin Hall effect

1. INTRODUCTION

Exciton-polaritons in semiconductor microcavities have been studied intensely both with respect to their intriguing fundamental physical properties[1–18] (for reviews see for example Refs. [13,17–19]), including polaritonic Bose condensation, and with respect to their potential in novel device designs.[20–23] The latter requires ways to control polaritonic systems, and all-optical control mechanisms are considered to be especially useful. In the following, we discuss and review our efforts to control various physical attributes. One of those attributes is the polariton density, which can be controlled by optical pump and control beams, utilizing optical instabilities that are based on four-wave mixing processes. Using a double-cavity design, which has two lower-polariton branches, we are able to pump the system in normal incidence and control the output direction with a combination of static system parameters and dynamical off-axis control beams. This allows for an efficient directional and low-energy switching of optical beams. A second example is the control of spin transport phenomena that leads to polarization patterns (or textures) in the far-field emission. We discuss the control of the so-called optical spin Hall effect. Utilizing again our double-cavity design, we are able to rotate the spin/polarization texture of the far field simply by changing the intensity of the pump beam. This effect is based on an optical manipulation of the polariton-spin orbit interaction, and may lead to novel applications in spinoptronic systems.

A semiconductor double-microcavity consists of two cavities,[24] each of which has one or more quantum wells embedded, as sketched in Fig. 1(a). The cavity photons and the excitons in the quantum wells are coupled and

---

Send correspondence to R. Binder: E-mail: binder@optics.arizona.edu, Telephone: 1 520 621 2892
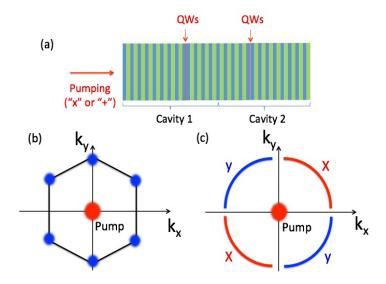
Figure 1. (a) A sketch of the semiconductor double-microcavity with a pump beam at normal incidence. Two quantum wells are embedded inside three distributed Bragg reflectors (DBR), which form two cavities. The (b) A schematic of the hexagonal intensity pattern spontaneously created by a normally incident light source with intensity above instability threshold. A two-spot pattern can also be created using different parameters. (c) A schematic plot of the optical spin Hall effect (OSHE) pattern created by a "+"-circularly polarized source. "x" and "y"-polarized polaritons are spatially separated due to the polariton spin-orbit interaction.

form exciton-polaritons. For a double-cavity, two upper and two lower polariton branches are formed, which is in contrast to one upper and one lower polariton branch in the case of a single-cavity. The extra polariton branches allow resonant frequency windows for the creation of directly pumped polaritons. An optical pump is in normal incidence to the cavity's surface. When the pump intensity is above a certain threshold, the nonlinear scattering of polaritons can lead to spontaneous symmetry breaking and pattern formation. Figure 1(b) shows a sketch of a possible hexagonal pattern observed in the far-field.

Another possible optical pattern that can be observed and controlled in a double-cavity is the optical spin Hall effect (OSHE) spin texture.[25–31] The OSHE is the formation of polarization/spin pattern of exciton-polaritons in an optically pumped semiconductor microcavity. The effect arises from the transverse-electric and transverse magnetic (TE-TM) splitting, which yields a polariton spin-orbit interaction. The spin-orbit interaction leads to an effective magnetic field that creates an anisotropic polarization texture of polaritons. The OSHE pattern with a linearly polarized ("x"-polarized) light source was recently shown in experiments,[31, 32] and is sketched in Fig. 1(c).

In the following, we will first discuss the theory of cavity photons and excitons in a semiconductor double-microcavity, and present numerical simulation results illustrating the formation of patterns and their optical control. In the next section, we will simplify the photon-exciton equations using the exciton-polariton picture and also formulate a pseudospin model. We will present results for the control of the OSHE pattern at different pump intensity using both the microscopic theory as well as the pseudospin formulation.

2. PATTERN FORMATION IN SEMICONDUCTOR DOUBLE-MICROCAVITIES

In this section, we describe one of the optical control mechanisms on the polariton patterns in a semiconductor double-microcavity as demonstrated in Ref. [24]. We start with considering the dynamics of the excitons and cavity photons in the two cavities. The equations describing the dynamics of the exciton and cavity photon fields

in the two cavities and quantum wells are

$$i\hbar\dot{E}_1^\pm = H_C E_1^\pm + H_\pm E_1^\mp - \Omega_C E_2^\pm - \Omega_X p_1^\pm + R_{\mathrm{pump},1}^\pm \tag{1}$$

$$i\hbar\dot{E}_2^\pm = H_C E_2^\pm + H_\pm E_2^\mp - \Omega_C E_1^\pm - \Omega_X p_2^\pm + R_{\mathrm{pump},2}^\pm \tag{2}$$

$$i\hbar\dot{p}_1^\pm = H_X p_1^\pm - \Omega_X(1 - 2A_{\mathrm{PSF}}|p_1^\pm|^2)E_1^\pm$$
$$+ T^{++}|p_1^\pm|^2 p_1^\pm + T^{+-}|p_1^\mp|^2 p_1^\pm \tag{3}$$

$$i\hbar\dot{p}_2^\pm = H_X p_2^\pm - \Omega_X(1 - 2A_{\mathrm{PSF}}|p_2^\pm|^2)E_2^\pm$$
$$+ T^{++}|p_2^\pm|^2 p_2^\pm + T^{+-}|p_2^\mp|^2 p_2^\pm \tag{4}$$

Here $E_i^\pm$ is the cavity photon field, and $p_i^\pm$ is the exciton field in the ith cavity ($i = 1, 2$ in a double-cavity) of plus $(+)$ and minus $(-)$ circular polarization. For cavity photons, $H_C = -\frac{\hbar^2}{4}\left(\frac{1}{m_{TM}} + \frac{1}{m_{TE}}\right)\nabla^2 + \hbar\omega_c - i\gamma_C$, and $H_\pm = -\frac{\hbar^2}{4}\left(\frac{1}{m_{TM}} - \frac{1}{m_{TE}}\right)\left(\frac{\partial}{\partial x} \mp i\frac{\partial}{\partial y}\right)^2$. For excitons, $H_X = -\frac{\hbar^2}{2m_X}\nabla^2 + \varepsilon_x - i\gamma_X$. $\hbar\omega_c$ and ε_x are the $\mathbf{k} = 0$ energies of the cavity mode and the 1s exciton, respectively. The two cavities have the same $\hbar\omega_c$ and ε_x as they are assumed to be identical. m_{TE} and m_{TM} are the cavity photon masses for the TE and TM modes, respectively. The spin-orbit coupling $H_\pm$ turns two units of spin into two units of orbital angular momentum and vice versa. It is non-zero when there is splitting in the TE and TM dispersion ($m_T E \neq m_T M$). m_X is the 1s heavy-hole exciton mass, which is assumed to be infinite in the range of interest. γ_C is the cavity loss rate and γ_X the exciton dephasing. Ω_X is the coupling strength between excitons and cavity photons in each cavity, and the photon fields in the two cavities are coupled with strength Ω_C. $R_{\mathrm{pump},1}^\pm$ and $R_{\mathrm{pump},2}^\pm$ are the effective pump sources in cavity 1 and 2, respectively.

The nonlinear couplings contain two parts: the phase space filling effect among the Fermionic constituents of the excitons (electrons and holes), denoted by A_{PSF}, and the effective interactions T^{++} and T^{+-}, in the co-circularly polarized and counter-circularly polarized exciton channels, respectively. Retardation (quantum memory) effects are neglected due to the quasi-monochromatic excitation conditions.

Steady state far-field patterns are obtained by numerically solving Eqs. (1)-(4) and Fourier transforming the cavity photon and exciton fields into transverse momentum (k) space. A continuous normally incident pump source, linearly polarized at 45°, with intensity above the instability threshold leads to a spontaneous hexagon formation in k-space, as shown in Fig. 2(b). The hexagon consists of two strong spots and four weaker spots, with the two strong spots orientated perpendicularly to the polarization of the pump. When the pump is tilted to the direction perpendicular to the pump polarization, as illustrated in Fig. 2(a), an anisotropy is introduced to the system. With a sufficiently strong anisotropy, the hexagon is destabilized and a two-spot pattern emerges, as shown in Fig. 2(c). Note that all detections are in the cross-polarized channel, which is the linear polarization at 135° in this case. Further examples of switching, including using a control beam, can be found in Ref. [24].

3. OPTICAL SPIN HALL EFFECT

To observe the OSHE pattern numerically with a "x"-polarized source, instead of computing the cavity photon and exciton fields as in Eqs. (1) - (4), we simplify the problem using the exciton-polariton picture taking into account only the two lower polariton branches, LP1 and LP2, as in:[33, 34]

$$i\hbar\frac{\partial}{\partial t}\psi_{LP1}^\pm = \tilde{H}_{\psi,1}\psi_{LP1}^\pm + \tilde{H}_{\pm,1}\psi_{LP1}^\mp + N_{\pm,1} + \tilde{R}_{\pm,1} \tag{5}$$

$$i\hbar\frac{\partial}{\partial t}\psi_{LP2}^+ = \tilde{H}_{\psi,2}\psi_{LP2}^+ + N_{+,2} + \tilde{R}_{+,2} \tag{6}$$

Here $\psi_{LP1}^\pm$ and $\psi_{LP2}^\pm$ are the polariton fields at the lowest polariton branch, LP1, and the second lowest polariton branch, LP2, in real space, respectively. The $k = 0$ energies of LP1 and LP2 polaritons are $\hbar\omega_{0,1}$ and $\hbar\omega_{0,2}$, respectively. We also make an assumption that $\psi_{\mathbf{k}}^{LP2-} = 0$ due to the $(+)$ polarized pump at energy equal to $\hbar\omega_{0,2}$. $\tilde{R}_{\pm,1/2}$ are the effective source terms on the two lower polariton branches and the assumption leads to $\tilde{R}_{-,2} = 0$. Moreover, $\tilde{H}_{\psi,1} = -\frac{\hbar^2}{2M_{LP1}}\nabla^2 + \hbar\omega_{0,1} - i\gamma$ and $\tilde{H}_{\psi,2} = -\frac{\hbar^2}{2M_{LP2}}\nabla^2 + \hbar\omega_{0,2} - i\gamma$. The spin-orbit
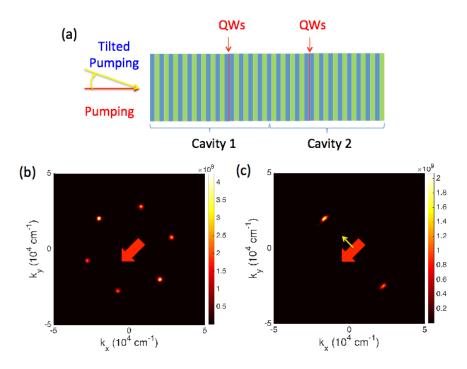
Figure 2. (a) A schematic illustration of the tilted pump (the tilt angle in the sketch is exaggerated for clarity). (b) A hexagonal intensity pattern is created by a normally incident polarized pump source, linearly polarized at 45°, with intensity above instability threshold. The polarization direction is indicated by the red arrow. The orientation of the two dominant spots in the hexagon is perpendicular to this polarization angle. The detection is cross-polarized with the pump, which is linearly polarized at 135°, in this case. (c) A two-spot pattern is observed when the pump is slightly tilted perpendicularly to the pump polarization direction, which is indicated by the small yellow arrow.

coupling is $\tilde{H}_{\pm,1} = -\frac{\hbar^2}{2m_{LP1}}\left(\frac{\partial}{\partial x} \mp i\frac{\partial}{\partial y}\right)^2$. Here $\frac{1}{M_{L1/2}} = \frac{1}{2}(\frac{1}{m_{1/2}^{TM}} + \frac{1}{m_{1/2}^{TE}})$ and $\frac{1}{m_{L1/2}} = \frac{1}{2}(\frac{1}{m_{1/2}^{TM}} - \frac{1}{m_{1/2}^{TE}})$ are the inverse sum of the effective TE and TM masses of LP1 and LP2, respectively. The nonlinear terms are

$$
\begin{aligned}
N_{\pm,1} &= (2\tilde{T}_{12}^{++} + \tilde{A}_{PSF,12} + \tilde{A}_{PSF,21})|\psi_{LP2}^{\pm}(\mathbf{r},t)|^2\psi_{LP1}^{\pm}(\mathbf{r},t) \\
&\quad +(\tilde{T}_{11}^{++} + \tilde{A}_{PSF,11})|\psi_{LP1}^{\pm}(\mathbf{r},t)|^2\psi_{LP1}^{\pm}(\mathbf{r},t) + (\tilde{T}_{12}^{++} + \tilde{A}_{PSF,12})\psi_{LP1}^{\pm}{}^{*}(\mathbf{r},t)\psi_{LP2}^{\pm}{}^{2}(\mathbf{r},t) \\
&\quad +\tilde{T}_{12}^{+-}|\psi_{LP2}^{\mp}(\mathbf{r},t)|^2\psi_{LP1}^{\pm}(\mathbf{r},t) + \tilde{T}_{11}^{+-}|\psi_{LP1}^{\mp}(\mathbf{r},t)|^2\psi_{LP1}^{\pm}(\mathbf{r},t) \quad\quad (7) \\
N_{+,2} &= (2\tilde{T}_{12}^{++} + \tilde{A}_{PSF,12} + \tilde{A}_{PSF,21})|\psi_{LP1}^{+}(\mathbf{r},t)|^2\psi_{LP2}^{+}(\mathbf{r},t) \\
&\quad +(\tilde{T}_{22}^{++} + \tilde{A}_{PSF,22})|\psi_{LP2}^{+}(\mathbf{r},t)|^2\psi_{LP2}^{+}(\mathbf{r},t) + (\tilde{T}_{12}^{++} + \tilde{A}_{PSF,21})\psi_{LP2}^{+}{}^{*}(\mathbf{r},t)\psi_{LP1}^{+}{}^{2}(\mathbf{r},t) \\
&\quad +\tilde{T}_{12}^{+-}|\psi_{LP1}^{-}(\mathbf{r},t)|^2\psi_{LP2}^{+}(\mathbf{r},t). \quad\quad (8)
\end{aligned}
$$

The coupling between polaritons are modified from the photon-exciton picture with $\tilde{T}_{11}^{++} = 2\beta_{11}^2 T^{++}$, $\tilde{T}_{11}^{+-} = 2\beta_{11}^2 T^{+-}$, $\tilde{T}_{22}^{++} = 2\beta_{22}^2 T^{++}$, $\tilde{T}_{12}^{++} = 2\beta_{11}\beta_{22} T^{++}$, $\tilde{T}_{12}^{+-} = 2\beta_{11}\beta_{22} T^{+-}$, $\tilde{A}_{PSF,11} = 4\beta_{PSF,11}^2 A_{PSF}\Omega_X$, $\tilde{A}_{PSF,22} = 4\beta_{PSF,22}^2 A_{PSF}\Omega_X$, $\tilde{A}_{PSF,21} = 4\beta_{PSF,21}^2 A_{PSF}\Omega_X$ and $\tilde{A}_{PSF,12} = 4\beta_{PSF,12}^2 A_{PSF}\Omega_X$. The coefficients are the

combinations of the Hopfield coefficients defined as

$$\beta_{11}^2 = \frac{\Omega_X^4}{4\left(\Omega_X^2 + (\varepsilon_x - \hbar\omega_{0,1} - \frac{\hbar^2 k_{res1}^2}{2M_{LP1}})^2\right)^2}$$

$$\beta_{22}^2 = \frac{\Omega_X^4}{4\left(\Omega_X^2 + (\varepsilon_x - \hbar\omega_{0,2})^2\right)^2}$$

$$\beta_{PSF,11}^2 = \frac{\Omega_X^3(\varepsilon_x - \hbar\omega_{0,1} - \frac{\hbar^2 k_{res1}^2}{2M_{LP1}})}{4\left(\Omega_X^2 + (\varepsilon_x - \hbar\omega_{0,1} - \frac{\hbar^2 k_{res1}^2}{2M_{LP1}})^2\right)^2}$$

$$\beta_{PSF,22}^2 = \frac{\Omega_X^3(\varepsilon_x - \hbar\omega_{0,2})}{4\left(\Omega_X^2 + (\varepsilon_x - \hbar\omega_{0,2})^2\right)^2}$$

$$\beta_{PSF,12}^2 = \frac{\Omega_X^3(\varepsilon_x - \hbar\omega_{0,2})}{4\left(\Omega_X^2 + (\varepsilon_x - \hbar\omega_{0,1} - \frac{\hbar^2 k_{res1}^2}{2M_{LP1}})^2\right)\left(\Omega_X^2 + (\varepsilon_x - \hbar\omega_{0,2})^2\right)}$$

$$\beta_{PSF,21}^2 = \frac{\Omega_X^3(\varepsilon_x - \hbar\omega_{0,1} - \frac{\hbar^2 k_{res1}^2}{2M_{LP1}})}{4\left(\Omega_X^2 + (\varepsilon_x - \hbar\omega_{0,1} - \frac{\hbar^2 k_{res1}^2}{2M_{LP1}})^2\right)\left(\Omega_X^2 + (\varepsilon_x - \hbar\omega_{0,2})^2\right)}, \tag{9}$$

where $k_{res1} = \sqrt{2M_{L1}\hbar\omega_{0,2}}/\hbar$. For detailed derivation please refer to Ref. [34].
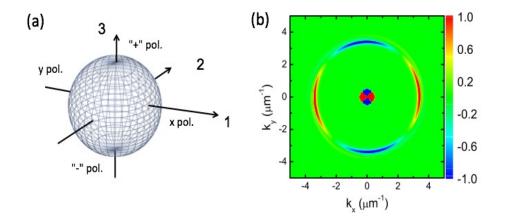

Figure 3. (a) The Poincare sphere representation of the pseudospin vector $\mathbf{S}$. The north and south pole correspond to "+" and "-"-polarized polaritons, respectively, while the positive and negative parts on the "S_1"-axis correspond to "x" and "y"-polarized polaritons, respectively. (b) Numerical results for $S_1(\mathbf{k})$ with a "+"-polarized normally incident source. The "x" (red) and "y" (blue) polarized polaritons are spatially separated into four quadrants in k-space. A further increase of the pump intensity will lead to a further rotation of the $S_1(\mathbf{k})$ pattern.[31] The data are normalized such that the maximum and minimum values are ± 1.

Before discussing the numerical simulation results of Eqs. (5) and (6), we introduce the pseudospin model.[31,35] The components of the pseudospin vector in k-space $\mathbf{S_k}$ are described by the Stokes parameters formed by the polariton wavefunctions:

$$\begin{aligned}
S_0(\mathbf{k}) &= |\psi_{\mathbf{k}}^{LP1+}|^2 + |\psi_{\mathbf{k}}^{LP1-}|^2 \\
S_1(\mathbf{k}) &= 2\text{Re}\left[\psi_{\mathbf{k}}^{LP1-*}\psi_{\mathbf{k}}^{LP1+}\right] \\
S_2(\mathbf{k}) &= -2\text{Im}\left[\psi_{\mathbf{k}}^{LP1-*}\psi_{\mathbf{k}}^{LP1+}\right] \\
S_3(\mathbf{k}) &= |\psi_{\mathbf{k}}^{LP1+}|^2 - |\psi_{\mathbf{k}}^{LP1-}|^2,
\end{aligned} \tag{10}$$

where $\psi_{\mathbf{k}}^{LP1\pm}$ is the spatial Fourier transform of $\psi_{LP1}^{\pm}$. The evolution of the pseudospin vector can either be obtained from the equations of motion for the polariton wave functions as detailed above, or from a phenomenological pseudospin model, given by the equations[31,35]

$$\dot{\mathbf{S}}(\mathbf{k}) = \mathbf{B}(\mathbf{k}) \times \mathbf{S}(\mathbf{k}) - \gamma_S \mathbf{S}(\mathbf{k}) + \mathbf{R}(\mathbf{k}) \tag{11}$$

with the effective magnetic field $\mathbf{B}_{\mathbf{k}}$, the decay term γ_S and a source term $\mathbf{R}(\mathbf{k})$. The pseudospin vector can be represented in the Poincare sphere as shown in Fig. 3(a). The north and south pole correspond to "+" and "-"-polarized polaritons, respectively, while the positive and negative parts of the S_1 axis correspond to mostly "x" and "y"-polarized polaritons, respectively. In other words, for a positive $S_1(\mathbf{k})$ the polarization state of the field is mostly "x", while for negative $S_1(\mathbf{k})$ it is "y".

We perform numerical simulations of Eqs. (5) and (6) with a "+"-circularly polarized light and observe the far-field polarization texture using $S_1(\mathbf{k})$. An example is shown in Fig. 3(b), which consists of four quadrants of mostly linearly polarized polaritons on the elastic circle. The polarization texture was shown to be rotated with an increase in pump intensity,[31] and in Fig. 4(a) we show the change in polarization of polaritons on the elastic circles at 0-degree under different pump intensity. Here we define the radial average of the Stokes parameters as

$$
\begin{aligned}
\bar{S}_1 &= \frac{I_{0,0} - I_{90,0}}{I_{0,0} + I_{90,0}} \\
\bar{S}_2 &= \frac{I_{45,0} - I_{135,0}}{I_{45,0} + I_{135,0}} \\
\bar{S}_3 &= \frac{I_{45,\pi/2} - I_{135,\pi/2}}{I_{45,\pi/2} + I_{135,\pi/2}}
\end{aligned}
\tag{12}
$$

where

$$I_{\phi_k,\eta} = \int_{k_1}^{k_2} k\,dk |\psi_k^{LP1x} \cos\phi_k + \psi_k^{LP1y} e^{i\eta} \sin\phi_k|^2 \tag{13}$$

is the radially integrated polariton density measured at angle ϕ_k. The range between k_1 and k_2 is determined by the thickness of the elastic circle so that further increase in the integration range does not change the $I_{\phi_k,\eta}$. Here, corrections to the Stokes parameters due to the small deviation of the emission from the surface normal has been neglected.
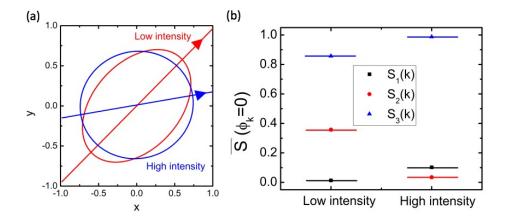

Figure 4. (a) The polarization ellipse of the far-field emission from polaritons at zero degrees on the elastic circle for low and high pump intensity. The azimuth angle of the polarization is rotated with a higher pump intensity. At the same time, the polarization is closer to a circle, i.e. the ellipticity is closer to $\pi/4$, with a higher pump intensity. (b) The three radially integrated Stokes parameters $\bar{S}_1$, $\bar{S}_2$ and $\bar{S}_3$ on the elastic circle at zero degrees for low and high pump intensities. The increase in $\bar{S}_1$ and decrease in $\bar{S}_2$ effect a change in the azimuth angle.

The ellipticity ϵ and the azimuth angle θ_{az} of the polarization of polaritons plotted in Fig. 4(a) is then given by

$$\epsilon = (1/2)\sin^{-1}\left(\bar{S}_3/\sqrt{\bar{S}_1^2 + \bar{S}_2^2 + \bar{S}_3^2}\right) \tag{14}$$

$$\theta_{\text{az}} = (1/2)\tan^{-1}\left(\bar{S}_2/\bar{S}_1\right). \tag{15}$$

The results in Fig. 4(a) show that the azimuth angle of the polarization is rotated and the polarization is closer to a circle, i.e. ellipticity is closer to $\pi/4$, with a higher pump intensity. These changes in the azimuth angle and ellipticity can be understood by studying the changes of $\bar{S}_{1/2/3}$ with low and high pump intensity. The values of $\bar{S}_{1/2/3}$ are shown in Fig. 4(b) for the two cases, and the change of ellipticity is coming from the increase of $\bar{S}_3$ in the high intensity case. From Eq. (14), a higher $\bar{S}_3$ weighting leads to a ellipticity ϵ closer to $\pi/4$. The change in azimuth angle comes from the combined effect of the increase in $\bar{S}_1$ and decrease in $\bar{S}_2$.

4. CONCLUSION

In conclusion, we have discussed two kinds of all-optical pattern control in a semiconductor double-microcavity, namely the hexagonal/two-spot intensity pattern and the OSHE spin texture, and showed that these patterns could be optically manipulated. In the intensity pattern case, a small tilt of pump can destabilize the hexagonal pattern and lead to the formation of a two-spot pattern. In the OSHE, increasing the pump intensity can lead to a rotation of the spin texture. These control mechanisms could be the fundamentals of future all-optical computation and communication utilizing polaritons in semiconductor microcavities.

ACKNOWLEDGMENTS

REFERENCES

[1] Kuwata-Gonokami, M., Inoue, S., Suzuura, H., Shirane, M., and Shimano, R., "Parametric scattering of cavity polaritons," *Phys. Rev. Lett.* **79**, 1341–1344 (1997).

[2] Fan, H., Wang, H., Hou, H. Q., and Hammons, B. E., "Biexcitonic effects in the nonperturbative regime of semiconductor microcavities," *Phys. Rev. B* **57**, R9451–R9454 (1998).

[3] Baars, T., Bayer, M., Forchel, A., Schaefer, F., and Reithmaier, J., "Polariton-polariton scattering in semiconductors microcavities: experimental observations of threshold density dependence," *Phys. Rev. B* **61**, R2409–R2412 (2000).

[4] Kwong, N. H., Takayama, R., Rumyantsev, I., Kuwata-Gonokami, M., and Binder, R., "Evidence of non-perturbative correlations in two-dimensional exciton systems in semiconductor microcavities," *Phys. Rev. Lett.* **87**, 027402–(4) (2001).

[5] Kwong, N. H., Takayama, R., Rumyantsev, I., Kuwata-Gonokami, M., and Binder, R., "Third-order exciton-correlation and nonlinear cavity-polariton effects in semiconductor microcavities," *Phys. Rev. B* **64**, 045316–(15) (2001).

[6] Savvidis, P. G., Baumberg, J. J., Stevenson, R. M., Skolnick, M. S., Whittaker, D. M., and Roberts, J. S., "Angle-resonant stimulated polariton amplifier," *Phys. Rev. Lett.* **84**(7), 1547 (2000).

[7] Huang, R., Tassone, F., and Yamamoto, Y., "Experimental evidence of stimulated scattering of excitons into microcavity polaritons," *Phys. Rev. B* **61**(12), R7854 (2000).

[8] Ciuti, C., Schwendimann, P., Deveaud, B., and Quattropani, A., "Theory of the angle-resonant polariton amplifier," *Phys. Rev. B* **62**(8), R4825 (2000).

[9] Stevenson, R. M., Astratov, V. N., Skolnick, M. S., Whittaker, D. M., Emam-Ismail, M., Tartakovskii, A. I., Savvidis, P. G., Baumberg, J. J., and Roberts, J. S., "Continuous wave observation of massive polariton redistribution by stimulated scattering in semiconductor microcavities," *Phys. Rev. Lett.* **85**(17), 3680 (2000).

[10] Houdre, R., Weisbuch, C., Stanley, R. P., Oesterle, U., and Ilegems, M., "Linear and non-linear behavior of cavity polaritons," *Physica E* **7**, 625–630 (2000).

[11] Saba, M., Ciuti, C., Bloch, J., Thierry-Mieg, V., Andre, R., Le Si Dang, Kundermann, S., Mura, A., Bongiovanni, G., Staehli, J. L., and Deveaud, B., "High-temperature ultrafast polariton parametric amplification in semiconductor microcavities," *Nature* **414**, 731 (2001).

[12] Whittaker, D. M., "Classical treatment of parametric processes in a strong-coupling planar microcavity," *Phys. Rev. B* **63**, 193305 (2001).

[13] Ciuti, C., Schwendimann, P., and Quattropani, A., "Theory of polariton parametric interactions in semiconductor microcavities," *Semicond. Sci. Technol.* **18**, 279 (2003).

[14] Savasta, S., Di Stefano, O., and Girlanda, R., "Many-body and correlation effects on parametric polariton amplification in semiconductor microcavities," *Phys. Rev. Lett.* **90**, 096403 (2003).

[15] Savasta, S., Di Stefano, O., and Girlanda, R., "Many-body and correlation effects in semiconductor microcavities," *Semicond. Sci. Technol.* **18**, S294 (2003).

[16] Langbein, W., "Spontaneous parametric scattering of microcavity polaritons in momentum space," *Phys. Rev. B* **70**, 205301 (2004).

[17] Baumberg, J. J. and Lagoudakis, P. G., "Parametric amplification and polariton liquids in semiconductor microcavities," *Phys. Stat. Sol. (b)* **242**, 2210 (2005).

[18] Keeling, J., Marchetti, F. M., Szymanska, M. H., and Littlewood, P. B., "Collective coherence in planar semiconductor microcavities," *Semicond. Sci. Technol.* **22**, R1 (2007).

[19] Sanvitto, D. and Timofeev, V., [*Exciton Polaritons in Microcavities*], Springer, Berlin (2012).

[20] Schumacher, S., Kwong, N. H., Binder, R., and Smirl, A. L., "Low intensity directional switching of light in semiconductor microcavities," *phys. stat. sol. (RRL)* **3**, 10–12 (2009).

[21] Dawes, A., "Towards a single-photon all-optical transistor," *Phys. Stat. Sol. Rapid Research Letters* **3**, A17 – A19 (2009).

[22] Shelykh, I., Kavokin, A., Rubo, Y. G., Liew, T., and Malpuech, G., "Polariton polarization-sensitive phenomena in planar semiconductor microcavities," *Semiconductor Science and Technology* **25**, 013001 –(47) (2010).

[23] Sanvitto, D. and Kena-Cohen, S., "The road towards polaritonic devices," *Nature Materials* **15**, 1061 – 1073 (2016).

[24] Ardizzone, V., Lewandowski, P., Luk, M. H., Tse, Y. C., Kwong, N. H., Lcke, A., Abbarchi, M., Baudin, E., Galopin, E., Bloch, J., Lemaitre, A., Leung, P. T., Roussignol, P., Binder, R., Tignon, J., and Schumacher, S., "Formation and control of turing patterns in a coherent quantum fluid," *Scientific Reports* **3**, 3016 (2013).

[25] Kavokin, A., Malpuech, G., and Glazov, M., "Optical Spin Hall Effect," *Physical Review Letters* **95**, 136601 –(4) (2005).

[26] Leyder, C., Romanelli, M., Karr, J. P., Giacobino, E., Liew, T., Glazov, M., Kavokin, A., Malpuech, G., and Bramati, A., "Observation of the optical spin Hall effect," *Nature Physics* **3**, 628 – 631 (2007).

[27] Langbein, W., Shelykh, I., Solnyshkov, D., Malpuech, G., Rubo, Y., and Kavokin, A., "Polarization beats in ballistic propagation of exciton-polaritons in microcavities," *Physical Review B* **75**, 075323 –(8) (2007).

[28] Manni, F., Lagoudakis, K. G., Paraiso, T. K., Cerna, R., Leger, Y., Liew, T. C. H., Shelykh, I. A., and Kavokin, A. V., "Spin-to-orbital angular momentum conversion in semiconductor microvacities," *Physical Review B* **83**, 241307(R) –(4) (2011).

[29] Maragkou, M., Richards, C. E., Ostatnicky, T., Grundy, A. J. D., Zajac, J., Hugues, M., Langbein, W., and Lagoudakis, P. G., "Optical analogue of the spin Hall effect in a photonic cavity," *Opt. Lett.* **36**, 1095 – 1097 (2011).

[30] Kammann, E., Liew, T., Ohadi, H., Cilibrizzi, P., Tsotsis, P., Hatzopoulos, Z., Savvidis, P., Kavokin, A., and Lagoudakis, P., "Nonlinear Optical Spin Hall Effect and Long-Range Spin Transport in Polariton Lasers," *Physical Review Letters* **109**, 036404 –(5) (2012).

[31] Lafont, O., Luk, S., Lewandowski, P., Kwong, N., , Leung, P., Galopin, E., Lemaitre, A., Tignon, J., Schumacher, S., Baudin, E., and Binder, R., "Controlling the optical spin Hall effect with light," *Applied Physics Letters* **110**, 061108 (2017).

[32] Kammann, E., Liew, T., Ohadi, H., Cilibrizzi, P., Tsotsis, P., Hatzopoulos, Z., Savvidis, P., Kavokin, A., and Lagoudakis, P., "Nonlinear optical spin hall effect and long-range spin transport in polariton lasers," *Physical Review Letters* **109**, 036404 (2012).

[33] Luk, S., Lewandowski, P., Kwong, N., Baudin, E., Lafont, O., Tignon, J., Leung, P., Chan, K., Babilon, M., Schumacher, S., and Binder, R., "Theory of controlled ballistic polariton transport in semiconductor double microcavities," To be published.

[34] Luk, S., Lewandowski, P., Kwong, N., Schumacher, S., and Binder, R., "Polariton formalism for semiconductor double microcavities," *SPIE Proceedings* **10102**, Ultrafast Phenomena and Nanophotonics XXI, 101020D (2017).

[35] Leyder, C., M.Romanelli, Karr, J. P., Giacobino, E., Liew, T. C. H., Glazov, M. M., Kavokin, A. V., Malpuech, G., and Bramati, A., "Observation of the optical spin Hall effect," *Nature Physics* **3**, 628 (2007).